Materials Science & Engineering C 106 (2020) 110172

Contents lists available at ScienceDirect

Materials Science & Engineering C

journal homepage: www.elsevier.com/locate/msec

Fabrication and characterization of polycaprolactone fumarate/gelatin-based nanocomposite incorporated with silicon and magnesium co-doped fluorapatite nanoparticles using electrospinning method

Tahmineh Ahmadi[a,b,*], Ahmad Monshi[c], Vajihsadat Mortazavi[d], Mohammad Hossein Fathi[c,d], Shahriar Sharifi[e], Mahshid Kharaziha[c], Leila Khazdooz[f], Amin Zarei[g], Majid Taghian Dehaghani[c]

[a] Department of Materials Engineering, Shahreza Branch, Islamic Azad University, P.O. Box: 86145-311, Shahreza, Iran
[b] Razi Chemistry Research Center (RCRC), Shahreza Branch, Islamic Azad University, Isfahan, Iran
[c] Department of Materials Engineering, Isfahan University of Technology, Isfahan 8415683111, Iran
[d] Torabinejad Dental Research Center, Department of Operative Dentistry, School of Dentistry, Isfahan University of Medical Sciences, Isfahan 8174673461, Iran
[e] W. J. Kolff Institute, Department of Biomedical Engineering, University Medical Centre Groningen, University of Groningen, P. O. Box 196, 9700 AD Groningen, the Netherlands
[f] Department of Science,Isfahan (Khorasgan) Branch, Islamic Azad University, Isfahan 81595-158, Iran
[g] Department of Science, Fasa Branch, Islamic Azad University, P.O. Box: 364, Fasa, Fars 7461713591, Fasa, Iran

ARTICLE INFO

Keywords:
Biodegradation
Gelatin
Nanocomposite fibrous membrane
Polycaprolactone fumarate
Silicon and magnesium co-doped fluorapatite

ABSTRACT

The aim of this study was to fabricate and characterize biodegradable polycaprolactone fumarate(PCLF)/gelatin-based nanocomposite incorporated with the 0, 5 and 10 wt% silicon and magnesium co-doped fluorapatite nanoparticles (Si-Mg-FA) membranes using electrospinning process for guided bone regeneration (GBR) and guided tissue regeneration (GTR) applications. Results demonstrated the formation of randomly-oriented and defect-free fibers with various fiber sizes depending on the Si-Mg-FA content. Moreover, incorporation of 5 wt% Si-Mg-FA significantly improved the mechanical strength (1.5times) compared to the mechanical strength of PCLF/gelatin membrane and nanocomposite with 10 wt% nanoparticles. There was no clear difference between degradation rate of PCLF/gelatin and PCLF/gelatin with 5 wt% nanoparticles at 7, 14 and 28 days of immersion in phosphate buffer saline while 10 wt% nanoparticles significantly increased biodegradation of PCLF/gelatin, and no cytotoxic effect of membranes was seen. Finally, scanning electron microscopy (SEM) micrographs of fibroblast cells cultured on the samples demonstrated that the cells were completely attached and spread on the surface of nanocomposites. In summary, PCLF/gelatin membranes consisting of 5 wt% Si-Mg-FA nanoparticles could provide appropriate mechanical and biological properties and fairly good degradation rate, making it appropriate for GTR/GBR applications.

1. Introduction

Nano composite membranes consisting of polymer matrix reinforced with ceramic nanoparticles are applied for guided bone regeneration (GBR) and guided tissue regeneration (GTR) applications. GTR/GBR membranes should be porous for cellular adaption and sufficient nutrient permission. Generally, the membranes are divided into two groups of bio-resorbable and non-resorbable [1]. Non-resorbable membranes such as expanded polytetrafluoroethylene (e-PTFE) should be removed after implantation via a second surgery, on the contrary bio-resorbable membranes such as collagen membranes not only do not need to be removed, but also should retain their structural integrity during healing. This attractive property has recently made bio-resorbable membranes promising for GTR/GBR applications [2]. However, fast degradation of the current resorbable membranes is the main challenge leading to degradation before complete tissue regeneration [3]. Consequently, various researches have been recently performed on different new membranes with controlled degradation rate and greater mechanical strength [4–6]. Between them, composite membranes containing natural polymers (such as gelatin, collagen, …) and synthetic polymers (such as poly(caprolactone) (PCL), poly(lactic acid) (PLA) and poly(glycolic acid) (PGA)) as well as bioactive nanoparticles could be good candidates for GBR and GTR applications [5,7–9]. Recently, polycaprolactone fumarate (PCLF), a derivate of PCL, has been

* Corresponding author at: Department of Materials Engineering, Shahreza Branch, Islamic Azad University, P.O. Box: 86145-311, Shahreza, Iran.
E-mail address: tahmineh.ahmadi@iaush.ac.ir (T. Ahmadi).

https://doi.org/10.1016/j.msec.2019.110172
Received 2 October 2018; Received in revised form 2 September 2019; Accepted 5 September 2019
Available online 06 September 2019
0928-4931/

introduced as a crosslinkable polymer for tissue engineering applications and drug delivery vehicles [10–13]. The mechanical, thermal, and rheological properties of PCLF, for instance, the tensile modulus, can vary from 0.87 to 138 MPa depending on the molecular weight of the polycaprolactone diol(commercially polycaprolactone diol of 530, 1200, or 2000 g/mol molecular weight are available) [10]. However, degradation rate of PCLF is not suitable for GTR/GBR membranes. Moreover, this polymer is not bioactive; therefore, its application with various degradable natural polymers and bioactive ceramics could be appropriate for GBR/GTR applications.

Among various kinds of bioactive bioceramics, hydroxyapatite [$Ca_{10}(PO_4)_6(OH)_2$, HA] is of great importance because of its similarity to mineral part of bone [14]. Bone mineral contains several ionic substitutions (e.g. Na^+, Mg^{2+}, Cl^-, SiO_4^{4-} and F^-) in comparison to synthesized HA [14–16]. Among them, magnesium is a crucial element for cellular and enzymatic reactions as well as bone mineralization [17,18]. In other words, silicon plays a critical role in bone calcification process, and doping the silicate groups into HA improves its osteoblast cell activity [19,20]. Bone cells proliferate more rapidly in the presence of soluble silicon [20], and fluoride ions replace hydroxyl groups in the apatite lattice structure, leading to the formation of fluorapatite (FA). Fluoride ions increase the stability of apatite and thereby decrease the solubility of FA in comparison to HA [21]. Fluorine ions suppress dental and bone caries [14]. Moreover, FA not only provides greater protein adsorption and cell attachment with respect to HA [22], but also promotes proliferation, morphology and differentiation of osteoblast cells [23]. In addition, other investigations show that silicon and magnesium substituted into the fluorapatite structure improve its bioactivity, cell proliferation and cell viability [24–26].

Various strategies have been applied to develop GTR/GBR membranes. Among them, electrospinning method is an effective approach which could provide a porous structure similar to the natural extracellular matrix [5,9]. However, a wide range of polymers such as PCLF are not electro-spinnable due to their low molecular weight. Blending these polymers with various types of suitable polymers with appropriate molecular weight is the main solution.

The aim of this research was to develop porous biodegradable nanocomposite membranes based on PCLF/gelatin incorporated with F, Mg and Si doped HA nano-powder using electrospinning process for GTR/GBR applications. Moreover, the structural, chemical and mechanical characteristics of nanocomposite membranes as well as in-vitro biodegradation and cell behavior were investigated in detail.

2. Materials and methods

The starting materials used in this investigation were silicon and magnesium co-doped fluorapatite nanoparticles (Si-Mg-FA), gelatin and polycaprolactone fumarate (PCLF).

2.1. Si-Mg-FA fabrication

In our previous study [27], Si–Mg–FA nano-powder (NP) was prepared using high-energy ball milling method. A mixture of phosphorous pentoxide (P_2O_5, Merck), calcium hydroxide ($Ca(OH)_2$, Merck), magnesium hydroxide ($Mg(OH)_2$, Merck), calcium fluoride (CaF_2, Merck) and silicon oxide (SiO_2, Sigma-Aldrich) powders was mechanochemically activated using a high energy planetary ball mill (Fretch Pulverisette 5) with a 125 mL zirconia vial and four zirconia balls with 20 mm in diameter at ambient temperature. Mechanochemical activation was performed using ball/powder mass ratio of 25:1 and rotation speed of 250 rpm. $Ca_{9.5}Mg_{0.5}(PO_4)_{5.5}(SiO_4)_{0.5}F_{1.5}$ was fabricated. As shown by transmission electron microscopy (TEM; CM120, Philips) image in Fig. 1, particles have agglomerated spherical shape morphologies with a mean diameter of about 30 nm.

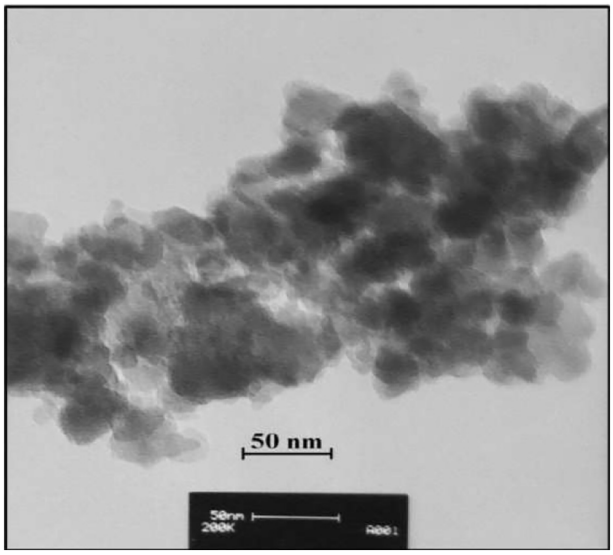

Fig. 1. TEM image of Si-Mg-FA nano-particles.

2.2. Preparation of PCLF macromer

PCLF macromer was primarily synthesized by condensation reaction of polycaprolactone (PCL) diols with fumaryl chloride (FuCl) in the presence of potassium carbonate according to the previously reported procedure [28]. All aforementioned chemicals and anhydrous dichloromethane (DCM) were purchased from Sigma–Aldrich Co. (Milwaukee, WI) and Merck Co. Prior to the reaction, a certain amount of PCL diol and potassium carbonate was dried under a vacuum at 60 °C and 100 °C for 24 h, respectively. Moreover, DCM was dried in the presence of calcium hydride. In addition, FuCl was distilled under vacuum at 161 °C. After drying and milling, 18 g (0.13 mol) of potassium carbonate was poured in a three-neck glass flask consisting of a reflux condenser under flowing nitrogen gas. Consequently, 225 g (0.11 mol) of PCL diol dissolved in 600 mL DCM was poured into the flask. The reaction vessel was heated to 40 °C by means of an oil bath, and then 17.2 g (0.11 mol) of freshly distilled FuCl dissolved in 20 mL methylene chloride was added drop-wise into the flask. After 12 h heating, the solution was centrifuged at 4000 rpm for 1 h to remove potassium carbonate, and then it was washed with de-ionized water. Subsequently, the resulting product was put in a rotary evaporator (heidolph) at 55 °C and at a pressure of 10 mmHg for 10 h. Finally, the resulting powder was placed in a vacuum oven at 30 °C for 24 h and subsequently stored in tight bottles in the dark at −20 °C until use.

2.3. Fabrication of PCLF/gelatin based nanocomposite membranes

Gelatin type A and 1-ethyl-3-(dimethyl-aminopropyl) carbodiimide hydrochloride (EDC) as a cross-linking agent were obtained from Sigma–Aldrich (St Louis, MO, USA).

Polymer solution of PCLF:gelatin with 1:1 weight ratio were prepared in 80% (v/v) acetic acid solution and mixed for 12 h at a final polymer concentration of 30 wt%. In order to cross-link the PCLF, the photo-initiator Irgacure 819(Merck Co) (5 wt% PCLF) dissolved in N-vinyl pyrrolidinone (Merck Co) (NVP, 20 wt% PCLF) was added to the PCLF solution. Subsequently, various concentrations of Si–Mg–FA nanopowders (0, 5 and 10 wt%) were added to polymer solution and mixed for 2 h in order to provide a uniform suspension. Electrical conductivity of solutions was evaluated by conductivity meter (JENWAY 4310). After 2 h ultrasonication, the suspensions were loaded into a 1 mL plastic syringe fitted with a stainless-steel blunt needle of 23 G in diameter using an infusion pump. The electrospinning parameters consisting of voltage (22 kV), feeding rate (2 mL/h) and the

working distance between the flat collector and needle (15 cm) were kept constant throughout the experiments. In order to crosslink the PCLF during electrospinning process, the electrospinning apparatus was placed under UVA light with a distance of 10 cm from the lamp head. The crosslinking process was continued for 5 h at 50 °C after electrospinning process. Moreover, in order to crosslink gelatin, electrospun membranes were immersed in 90% (v/v) ethanol solution containing 75 mM EDC for 12 h at 5 °C. After crosslinking, the membranes were rinsed with phosphate buffer solution (PBS, Gibco, USA) to remove the residual crosslinking agent. Finally, the membranes were put under a vacuum desiccator overnight. In order to evaluate the role of PCLF in the properties of the membranes, pure gelatin fibrous membrane (G membrane) was similarly fabricated via electrospinning process. According to the concentration of Si–Mg–FA nanopowder in the PCLF/gelatin membranes (0, 5 and 10 wt%), the samples were named P-G, P-G-5NP and P-G-10NP.

2.4. Characterization of PCLF/gelatin based nanocomposite membranes

The morphology of the fibrous membranes was examined with scanning electron microscopy (SEM; Philips XL30). Before observation, the samples were sputter coated with Au in a sputter coater (Bal-Tec SCD 005) to prevent sample charging during imaging. Based on the SEM images, the average diameter of electrospun fibers was determined by measuring the single arbitrarily selected fibers using image analysis software (Image J, National Institutes of Health, USA). Moreover, the morphology and spatial distribution of the Si–Mg–FA nanoparticles within the nanocomposites membranes were examined by transmission electron microscopy (TEM, Philips EM208S). The TEM samples were prepared by depositing the as-spun fibers on carbon-coated copper grids. The accelerating voltage was 100 kV.

Fourier transform infrared spectroscopy (FTIR, Bomem MB100) was performed over a range of 400–4000 $cm^{-1}$and resolution of 1 cm^{-1} to verify the chemical composition (functional groups) of the PCLF and composites. Moreover, x-ray diffraction (XRD) patterns of the samples were performed by a Philips X'Pert x-ray diffractometer with CuK_{α} radiation ($\lambda = 0.1542$ nm) over a 2θ range of 10–60° (time per step: 1 s and step size: 0.02°) under a voltage of 40 kV and a current of 30 mA. The crystalline phases were identified by comparing the obtained experimental patterns with the JCPDS cards.

2.5. Evaluation of wettability

The hydrophilicity of the membranes was measured using the static sessile drop technique. In this way, approximately 2 μl of water (pH = 7.0) was injected different sites of membranes and its contact angle was determined using video contact angle measurement setup (VCA Optima, AST Inc.) after a static time of 20 s. The reported values are presented as mean ± standard deviation.

2.6. Evaluation of PCLF crosslinking

In order to measure the amounts of crosslinked polycaprolactone fumarate, different percentages of Irgacure (2, 5, 15 wt% PCLF) were used as optical initiator materials. Moreover, NVP (20 wt% PCLF) was used as an active diluent. After the crosslinking process, the samples were precisely weighed (W_0), and then they were incubated in dichloromethane (DCM) for 24 h at room temperature. Subsequently, the samples were taken out from DCM, dried and weighed (W_1). Uncrosslinked PCLF was dissolved in DCM. The weight loss of samples (W_{loss}) was calculated according to the following equation:

$$\text{Weight loss}\ (\%) = ((W_1 - W_0)/W_0) \times 100 \quad (1)$$

2.7. Evaluation of mechanical properties

According to ASTM D638-10 standard, the mechanical properties of the samples (P-G, P-G-5NP and P-G-10NP) were evaluated by uniaxial tensile testing (Zwickmaterialpufung 1446) at a cross-head speed of 1 $mm.min^{-1}$ with a 10 N load cell. The samples were carefully cut into the rectangular dimension of 10 mm width and 50 mm length. Ultimate tensile strength (UTS), elastic modulus (E) and strain at failure (%) were calculated from the stress-strain curves. Five samples were tested for each type of electrospun membranes, and the results are reported as means ± standard deviation (SD).

2.8. Degradation rate evaluation

In vitro degradation behavior of membranes was studied by measuring their weight loss in phosphate buffered saline (PBS) solution according to ASTM F1635-95. In this regard, the membranes with the dimension of 20 mm × 20 mm × 2 mm (length, width, thickness) were precisely weighed (W_0), and then they were incubated in PBS for 1, 4, 7, 14, 21 and 28 days in a continuous shaking water bath at 37 °C. At predetermined periods, the samples were rinsed 3 times with distilled water and dried at room temperature for 4 days. The weight loss of samples (W_{loss}) was calculated according to the following formula:

$$\text{Weight loss}\ (\%) = ((W_d - W_0)/W_0) \times 100 \quad (2)$$

Moreover, the morphology of the membranes, after soaking for 7 days, was investigated using SEM technique.

2.9. Cell culture

The cell-membrane interaction was investigated using Mouse fibroblast cells (L929 Cell, purchased from the Pasture Institute of Iran). Before cell seeding, the samples were sterilized with 70% ethanol, and subsequently washed with PBS, followed by irradiation under UV for 8 h. Cells were grown in Dulbecco's modified Eagle's medium (DMEM) containing 10% (v/v) fetal bovine serum (FBS) supplemented with 1% penicillin (v/v) and 100 units/mL penicillin-streptomycin at 37 °C with 5% CO_2 in a humidified incubator. After reaching 80% confluency, the cells were detached with trypsin and then 2×10^4 cells were seeded on sterilized samples in a 24-well plate. Borosilicate glass cover slips with no sample were used as a reference substrate in experiments.

MTT (3-(4,5-Dimethylthiazol-2-yl)-2,5-diphenyltetrazolium bromide, a tetrazole) assay was employed to evaluate the cytotoxicity of the samples. In this way, after 3 days of culture, the MTT solution was added to each well and the plates were incubated for 4 h. After that, 250 μL dimethyl sulfoxide (DMSO) was added to each well to dissolve the formazan crystals formed by living cells. The plates were then gently shaken for 25 min and the optical density (OD) was read using ELISA instrument at 540 nm (all materials were purchased from Sigma and Merck Companies).

The morphology of fibroblast cells cultured on the membranes was studied by SEM imaging. After 3 days of culture, the cells were fixed in 2.5% glutaraldehide for 3 h at room temperature, dehydrated in a graded series of ethanol solution (50%, 70%, 80%, 90% and absolute ethanol) and finally air-dried. In order to study cell morphology, cell cultured samples were gold coated and studied by SEM (Philips XL30, USA).

2.10. Statistical analysis

Data were presented in mean ± standard deviation (SD). Statistical significance was measured by using one-way ANOVA analysis and comparisons were made by Tukey's post-hoc test using GraphPad Prism Software (V.5). A P-value < 0.05 was taken to be significant.

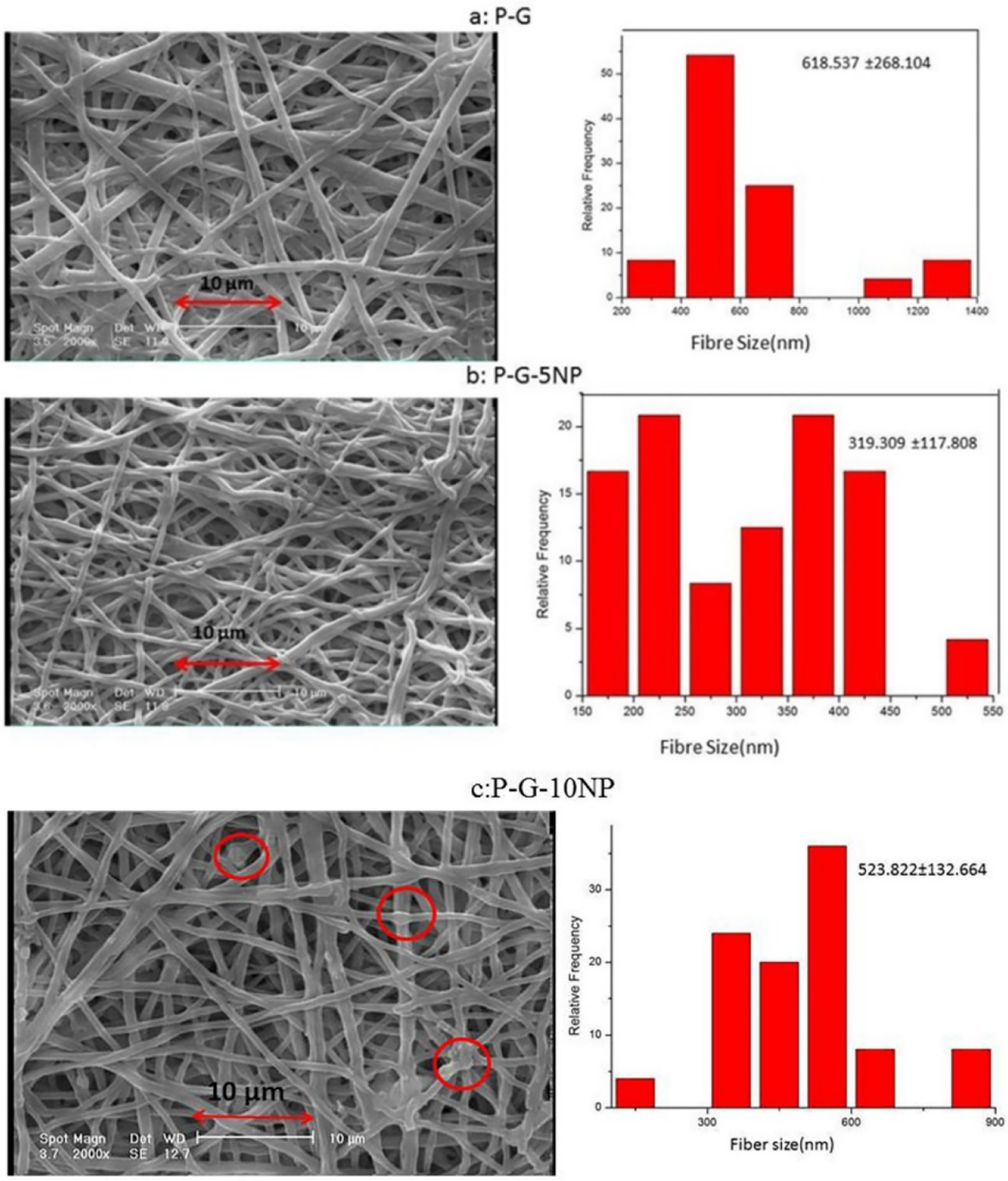

Fig. 2. SEM images and fiber size distribution of (a) P-G, (b) P-G-5NP and (c) P-G-10NP membranes. The red circles reveal the agglomeration of nanoparticles. (For interpretation of the references to colour in this figure legend, the reader is referred to the web version of this article.)

3. Results and discussion

3.1. Characterization of PCLF/gelatin based nanocomposite membranes

SEM images of the electrospun P-G, P-G-5NP and P-G-10NP fibrous membranes are presented in Fig. 2. All membranes consisted of randomly-oriented and bead-free fibers with uniform and smooth surfaces. However, it could be found that the morphology of fibers including diameter, porosity and surface structure was influenced by many processing parameters such as viscosity of suspension determined by polymer concentration and additives, spinning voltage, solution feeding rate, needle inner size and working distance in the electrospinning apparatus. Here, as mentioned in Section 2.3, voltage, working distance, feeding rate and needle size were constant. According to Fig. 2, the average size of fibers was reduced from 618 ± 268 nm (in P-G sample) to 319 ± 117 nm (in P-G-5NP) and 523.822 ± 132.664 nm (in P-G-10NP). Our results showed that incorporation of 5 wt% Si–Mg–FA nanoparticles resulted in reduced fiber diameter and enhanced porosity (up to 5%), more nanoparticles(10%) resulted in enhanced average fiber diameter due to the agglomeration of nanoparticles in comparison to 5% nanoparticles. Agglomerated nanoparticles were shown in Fig. 2(c) with the average size of 1172.570 ± 447.310 nm. Similarly, previous investigations revealed that less viscosity resulted in a thinner fiber diameter [29–31]. In fact, the less viscosity solutions make it easy to force through the syringe needle of the apparatus, increasing the flow rate. Electrical conductivity of polycaprolactone fumarate/gelatine solution is 639 µs/cm. when 5 wt% nanoparticles were added to the polymer solution, electrical conductivity doubled. Addition of 10 wt% nanoparticles to polymer solution increased conductivity (2.6 times polymer solution), in this case nanoparticles were agglomerated and settled down very soon. Apatite nanoparticles have ionic bond properties and Zong et al. [32] pointed out that the addition of some salt with ionic bond properties into a polymer solution resulted in a higher charge density on the

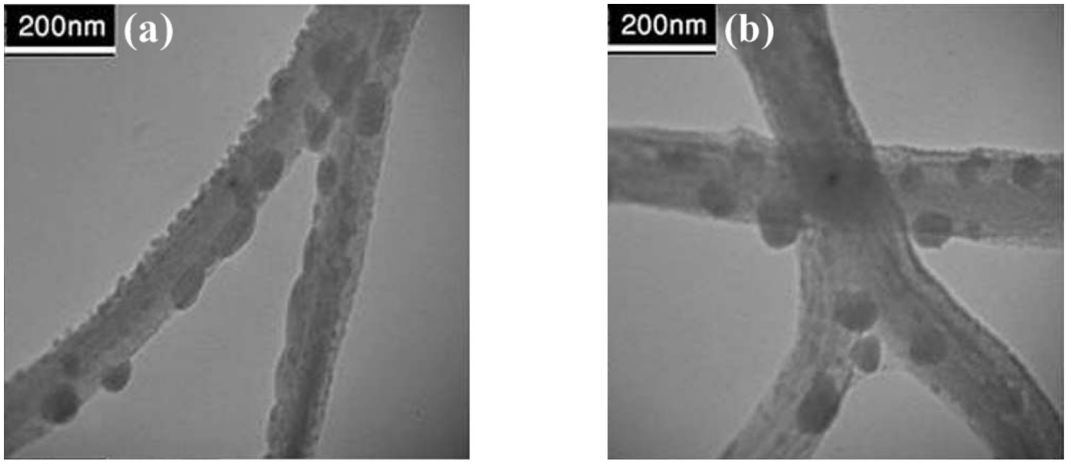

Fig. 3. TEM images of P-G-5NP membrane showing the distribution of Si-Mg-FA nano-powders into PCLF/Gelatin matrix.

surface of the solution jet. More electric charges to the jet led to higher elongation forces, resulting in a thinner fiber diameter.

The spatial particle size distribution and morphological shape of Si–Mg–FA nanoparticles embedded in the fibers was also evaluated by TEM imagining. The TEM micrographs of P-G-5NP (Fig. 3) showed that spherical Si–Mg–FA nanoparticles were well dispersed uniformly along the fibers with an average diameter of 50 nm. Uniform nanoparticle distribution is essential for the improvement of mechanical and biological properties of the membranes [33]. Totally, as discussed earlier, the mechanical properties of a particle reinforced membrane are dependent on various factors such as reinforcement volume fraction, shape of particles, spatial distribution of particles, pores and bead defects within the matrix of the membrane. For instance, beaded fibers relatively show lower mechanical strength in comparison to smooth surface fibers [34]. On the other hand, various important factors such as surface topography and energy as well as porosity influenced the cell adhesion and proliferation. It was reported that higher surface area led to the improvement of cell attachment and proliferation [35,36]. It is apparent from Fig. 2 that the pore shape is generally elongated and connected to other pores. These pores within the membranes, with different orientations resulting from random orientation and interconnection of the fibers, could provide special topography for cell attachment and proliferation.

FTIR spectroscopy was also applied to identify the presence of different functional groups in the samples. Fig. 4 shows the FTIR spectra of

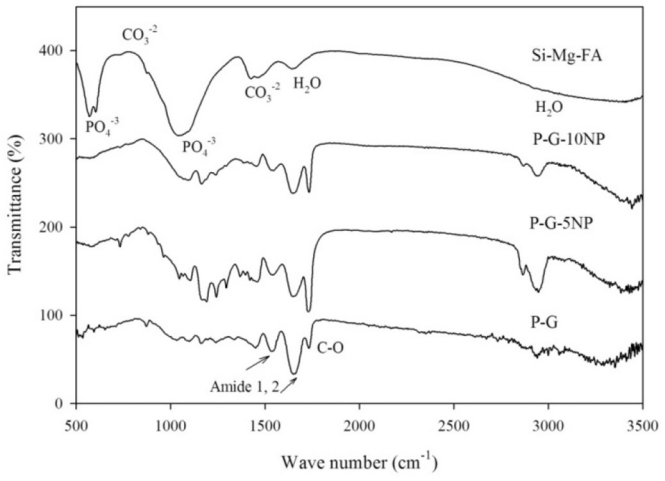

Fig. 4. FTIR spectra of Si-Mg-FA nano-powders as well as P-G, P-G-5NP and P-G-10NP membranes.

Si-Mg-FA nano-powder, P-G, P-G-5NP and P-G-10NP membranes. The FTIR spectrum of P-G membrane consisted of two characteristic absorption peaks at about 1562 cm^{-1} and 1650 cm^{-1} attributed to amide I band and II band of the gelatin, respectively. The former was related to the stretching vibrations of C—O bond of peptide linkages in the protein and the latter arose from coupling of the N—H bond in plane bending and stretching of the C—N bonds. In addition, the absorption peaks located at 1728 cm^{-1} and 2937 cm^{-1} corresponded to the stretching of ester functional groups and methyl group of PCLF/gelatin, respectively. It is worth mentioning that for pure gelatin, a broad band between 3400 cm^{-1} and 3440 cm^{-1}, assigned to an available N—H stretching vibration, was shifted to lower frequencies when the N—H group of a peptide bond was involved in a hydrogen bond. Furthermore, in the polyester/gelatin structure in comparison to gelatin structure, a less wave number and less amplitude were found, revealing involved N—H functional group of shorter peptide fragments in hydrogen bonding regarding the polyester/gelatin structure. Formation of new covalent intermolecular cross-links may also be observed during electrospinning of gelatin [37,38]. In other words, FTIR spectrum of Si–Mg–FA nanopowder represented the characteristic structural bands of fluorapatite (FA). The bands at 576 cm^{-1} and at 1043 cm^{-1} were assigned to the bending modes and the asymmetrical stretching peaks of PO_4^{-3}, respectively. Moreover, carbonate peaks at 740 cm^{-1} for the bending modes, at 884 cm^{-1} for vibration band and a doublet at 1433 cm^{-1} and 1468 cm^{-1} for the asymmetrical stretching revealed that some carbonates groups were substituted into PO_4^{-3} sites of apatite lattice [39,40]. Moreover, a clear band at 1650 cm^{-1} and a broad band between 3000 cm^{-1} and 3600 cm^{-1} were related to the water adsorbed in apatite lattice in the sample and/or absorbed in the KBr pellet [41]. Previous investigations revealed that the FTIR spectrum of the HA (hydroxyapatite) displayed clear bands at 631 cm^{-1} and 3573 cm^{-1} attributed to the structural hydroxyl groups which were due to the OH^{-1} immersed in an infinite chain of OH^{-1} [42,43]. Here, as the fluoride ion was incorporated into the apatite lattice, this chain was disturbed by F^{-1} in FA structure, leading to the disappearance of these two bands in the spectrum [44]. In addition, FTIR spectra of nanocomposite membranes consisted of all main characteristic peaks of polymers although the peak intensities were changed as a result of the dispersion of Si-Mg-FA nano-particles in the PCLF/gelatin polymer matrix. Furthermore, the intensity of Si-Mg-FA absorbance bands enhanced with increasing weight ratio of nanoparticles in polymer matrix. It is worth mentioning that as already mentioned, there are peaks corresponding to carbonate ions substituted in apatite lattice in all samples. Due to the absorption of carbon dioxide from the atmosphere [39,45] and calcination in air or presence of some solvent precursors [41], this carbon content resulted in more similarity between synthetic

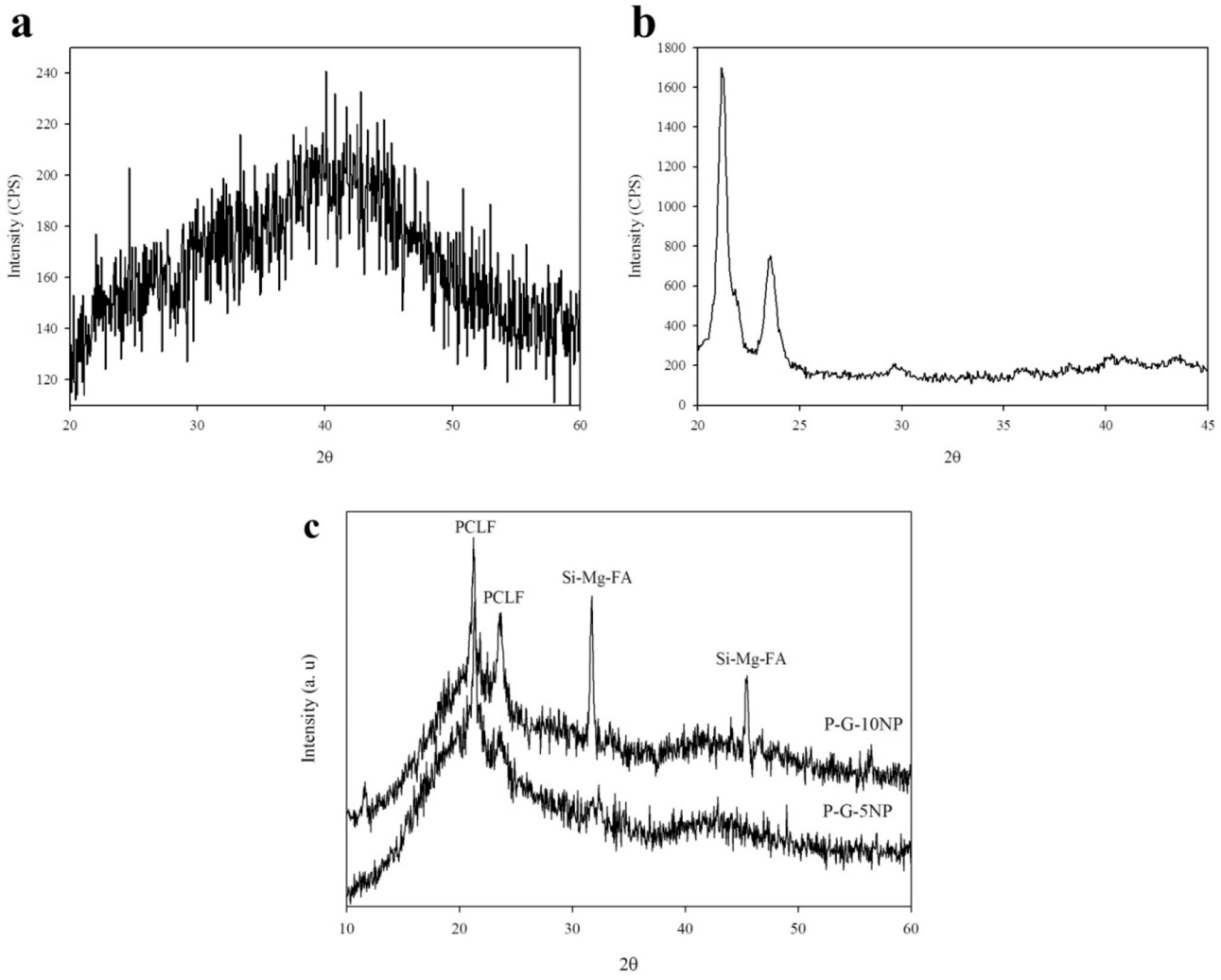

Fig. 5. XRD patterns of (a) gelatin, (b) PCLF and (c) P-G-5NP and P-G-10NP membranes.

apatite and the biological apatite [18].

In order to confirm the presence of nanoparticles in the polymer matrix, XRD patterns of nanocomposites as well as pure polymers and nanopowder were investigated (Fig. 5). The XRD pattern of gelatin (Fig. 5a) consisting of two broad peaks centered at $2\theta = 25^{\circ}$ and $2\theta = 40^{\circ}$ without any crystalline peaks, confirmed the disorderly and amorphous structure of this polymer. This result was in agreement with previous researches [46,47] although there are some investigations indicating that gelatin could be crystallized to some extent under special conditions. For instance, Ki et al. [48] investigated the effect of formic acid on the crystal structure and crystallinity of gelatin film and electrospun nanofiber. They found that although gelatin powder gives a typical XRD pattern of gelatin crystalline structure originating from a-helix and triplehelical structure, amorphous structures were observed for the film and electrospun nanofiber from gelatin–formic acid solution. In another work done by Pal et al. [49], the percent crystallinity of gelatin membrane was found to be 9.84%. XRD pattern of PCLF (Fig. 5b) also consisted of a weak background and strong peaks at $2\theta = 21.3^{\circ}$ and $2\theta = 23.7^{\circ}$ attributing to the amorphous and crystalline phases in its structure, respectively. Reflections peaks at $2\theta = 21.3^{\circ}$ and 23.7° related to the (110) and (200) crystallographic planes, respectively, were close to orthorhombic PCL reflections [50]. Polymeric architecture of PCLF from linear to branch depending on molecular weight suppresses the crystallization completely. [51]. Here, the percentage of crystallinity of synthesized PCLF synthesized from PCL diol 2000 at this research, calculated by the ratio of the crystalline and amorphous reflections indicated in Fig. 5b was equal to 83.5%. XRD patterns of P-G-5NP and P-G-10NP membranes (Fig. 5c) consisted of all characteristic peaks and amorphous background corresponding to gelatin, PCLF polymers and Si-Mg-FA nanoparticles. As expected, the intensity of the peaks corresponding to Si-Mg-FA nanoparticles enhanced distinctly with an increase in nano-particles content from 5 wt% to 10 wt% in the membranes.

3.2. Evaluation of the degree of cross-linking of polycaprolactone fumarate

To evaluate the cross-linking degree of polycaprolactone fumarate, different percentages of irgacure were used as an optical initiator material. The sample with 15 wt% irgacure had the best result for PCLF crosslinking. NVP was used as an active diluent. PCLF is an unsaturated polyester and needs an active diluent for crosslinking. About medical polyesters, in order to change the additional unreactant monomers to biocompatible polyvinyl pyrrolidyn, NVP is used as a diluent monomer [52,53]. Since PCLF molecule is great and does not have much mobility, it cannot be cross-linked to a high degree of conversion at low temperature. For this purpose, after electrospinning and exposing UV light simultaneously, the samples were also exposed to UV light at 50 °C for 5 h. The higher amount of crosslinking led to the decrease in its solubility in DCM and lower weight loss. The membrane of P-G-5NP with 15 wt% irgacure has the least weight loss (19.12 ± 0.97), meaning that the 61.76% PCLF had been cross linked.

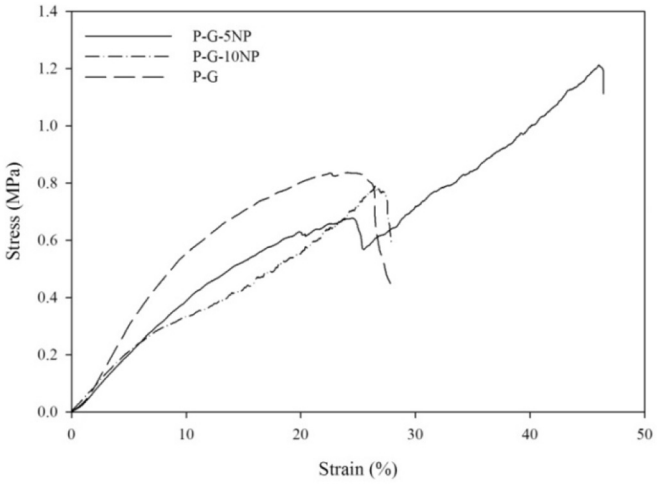

Fig. 6. Tensile stress-strain curves of P-G, P-G-5NP and P-G-10NP membranes.

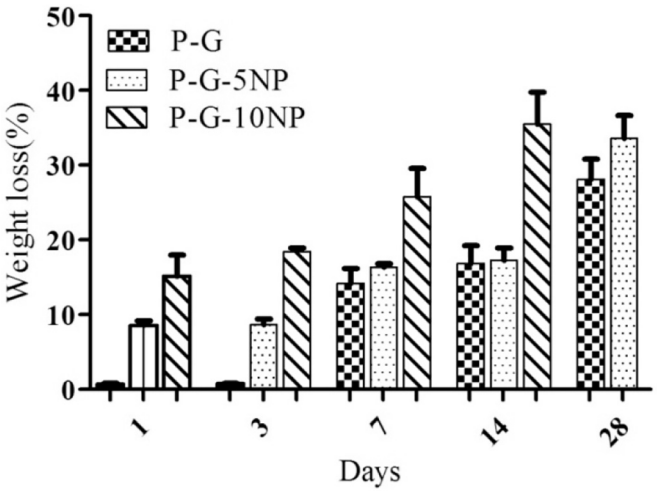

Fig. 7. The weight loss of the P-G, P-G-5NP and P-G-10NP membranes as a function of immersion time in PBS.

3.3. Evaluation of mechanical properties

Stress-strain curves of P-G, P-G-5NP and P-G-10NP samples are shown in Fig. 6. All samples revealed similar stress-strain trends consisting of an initial linear region where the samples obeyed Hook's law, a yield point where the curves deviated from the linear relationship followed by a plastic region up to a peak stress and finally a stress drop where the samples fracture under tensile force. The most important mechanical properties calculated from the curves including elastic modulus (E), ultimate tensile strength (UTS) and strain at break (%e) are listed in Table 1. It could be concluded that while incorporation of 5 wt% nanoparticles resulted in enhanced strain at break and UTS, increasing amounts of nanoparticles upon 10 wt% reduced the mechanical properties. According to previous results, the mechanical properties of the polymer matrix composites filled with nanoparticles could be influenced by some fixed or variable parameters such as chemical composition of matrix and filler and interaction between them, membrane architecture, morphology, size and dispersion of nanoparticles [54–56]. Among aforementioned parameters, here, distribution of nano-particles, fiber diameter and interaction between nano-particles and polymer chains play important roles in final mechanical properties of nano-composites. The improved mechanical properties of the membranes at lower nanoparticles content could be attributed to the energy-dissipating mechanism introduced by deposition of nanoparticles between entangled and random fibers [56]. According to this mechanism, orientation and alignment of nanoparticles as a result of the mobility of nano-particles under tensile stress led to the mechanical interlocking through making temporary cross-link among fibers. However, reduced mechanical properties of membranes at higher nanoparticle content might be due to the poor distribution of the nanoparticles leading to their agglomeration along the fiber. Agglomerated nano-particles acted as stress concentration sites behaving as defects [54]. On the other hand, in a research conducted by Wong et al. on poly (ε-caprolactone) [55], it was found that the modulus and strength of the fibrous membranes enhanced as the fiber diameter was reduced, and this effect becomes more predominant in the case of fibers with less than about 700 nm. Although their finding is in agreement with an increase in elastic modulus in our research because the increase in nano-particles percent resulted in a decrease in the mean fiber diameter, it seems to be in contradiction to lower strength.

Table 1
Mechanical properties of P-G, P-G-5NP and P-G-10NP samples.

Sample	Modulus (MPa)	Strain at break (%)	Ultimate tensile stress (MPa)
P-G	2.7 ± 0.2	24.0 ± 1.4	0.8 ± 0.1
P-G-5NP	2.0 ± 0.1	42.0 ± 3.0	1.3 ± 0.1
P-G-10NP	2.5 ± 0.5	26.5 ± 1.5	0.8 ± 0.1

3.4. In vitro biodegradation evolution

Fig. 7 shows weight loss of the P-G, P-G-5NP and P-G-10NP samples over a 4-week period. Results showed that the degradation rate of samples depended on the nanoparticle contents. Although all samples revealed a slow weight loss until 14 days, a dramatic decrease in weight was estimated afterwards. There was no clear difference between degradation rate of PCLF/gelatin and PCLF/gelatin with 5 wt% nanoparticles at 7, 14 and 28 days of immersion in phosphate buffer saline while 10 wt% nanoparticles significantly increased biodegradation of PCLF/gelatin. Among various samples, P-G-10NP membrane revealed the fastest degradation compared to others so that it did not maintain its structural integrity and was quite impossible to weigh after 28 days of immersion. The SEM micrographs of P-G, P-G-5NP and P-G-10NP, after immersion in PBS solution for one week, are presented in Fig. 8. Results showed that the morphology of all membranes was changed due to the swelling of the fibers. In addition, swelling of the fibers occurs more intensely for P-G-10NP, leading to the rupture of some fibers. Previous investigations revealed that the degradation of PCLF and gelatin was due to the uptake of water followed by the hydrolysis of ester bonds and carboxyl-amino groups, respectively [57–59]. Moreover, faster degradation rate of P-G-10NP compared to other samples might be related to the improvement of hydrophilicity of the membranes with increasing nano-particles. Results showed that water contact angles of P-G, P-G-5NP and P-G-10NP samples were 32.2°, 26.1° and 24.0°, respectively, indicating lower contact angles with increasing nanoparticles. Furthermore, as already mentioned, the increase in nanoparticles concentration resulted in a decrease in mean fiber diameter and an increase in porosity. Thinner fiber diameter and higher porosity percentage which result in larger surface area and more nano-particles exposed to PBS solution accelerate the degradation and the weight loss of the samples.

3.5. In vitro cell behavior

The MTT assay was employed to determine the proliferation of cells cultured on the P-G, P-G-5NP, P-G-10NP and control for 72 h. According to Fig. 9, no samples revealed any in vitro toxicity to the cells. According to the statistical analysis carried out by analysis of variance and $p < 0.05$, there was no significant difference in cell

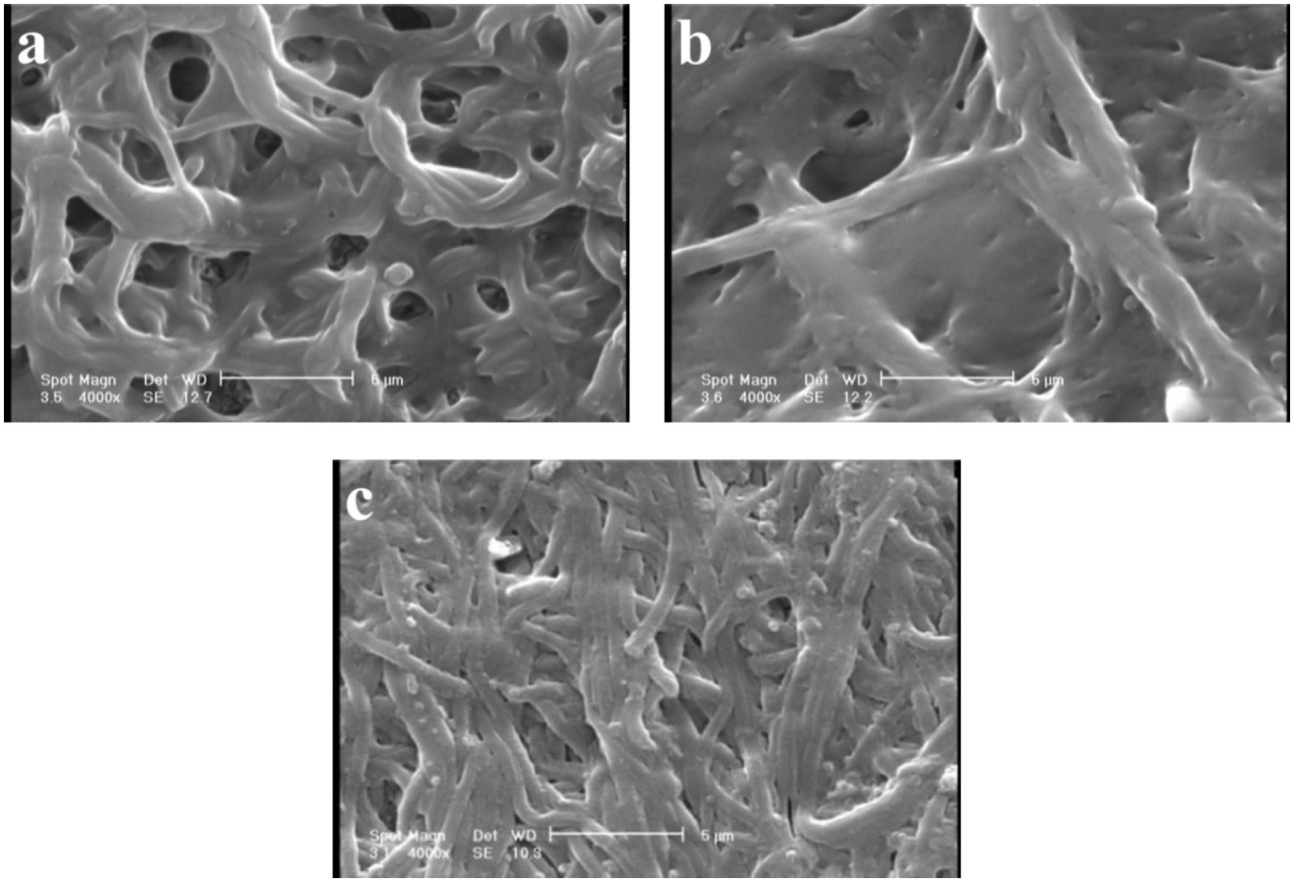

Fig. 8. SEM images of (a) P-G (b) P-G-5NP and (c) P-G-10NP after 7 days of immersion in PBS.

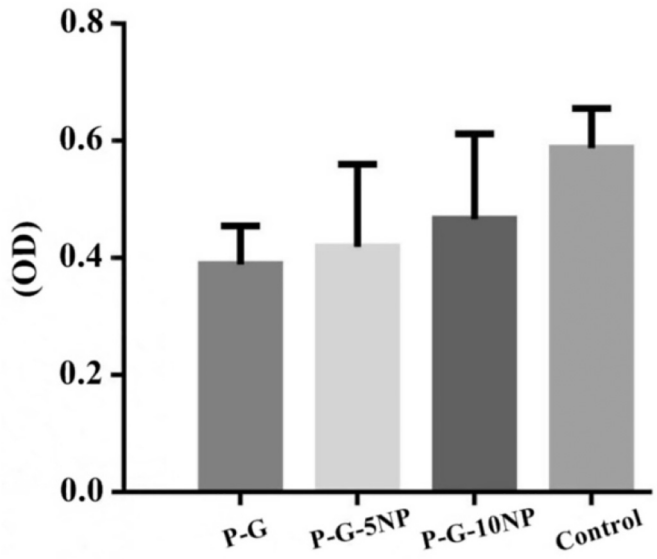

Fig. 9. MTT assay on the L929 fibroblast cell cultured on P-G, P-G-5NP, P-G-10NP and control, after 72 h culture.

proliferation between samples and control.

SEM micrographs of L929 fibroblast cells cultured on P-G and P-G-5NP membranes are presented in Fig. 10. Well cell attachment was evident for all samples; it seems that there were more cells on P-G-5NP than P-G membrane. The cells on the P-G-5NP were well spread and displayed flattened sheet morphologies. Attachment and proliferation of cells on the surface and inside the material for samples might be related to the porous structure of the membranes. Porous architecture with a wide variety of pore shapes and sizes provides a more desirable environment for cell attachment and proliferation [60]. In addition, the membranes consist of gelatin as the main component. Previous studies have shown that gelatin containing many integrin binding sites (such as the Arg-Gly-Asp (RGD) sequence which is the cell attachment site) improves cell attachment and cell proliferation [37,61]. Distributed nano-particles in P-G-5NP sample led to higher wettability to P-G sample. As mentioned before, contact angle decreased with an increase in nanoparticles indicating higher wettability. It has been shown that more surface roughness and higher wettability promote cell adhesion, spreading and proliferation [62]. Moreover, the presence of nano-particles in P-G-5NP membrane led to Si and fluoride ions release in the cell culture medium. Previous reports have shown that these ions enhance cell attachment and subsequent cell activities [45,63]. As already mentioned, P-G-5NP nanocomposite was stronger than P-G membrane as indicated by higher ultimate tensile stress. This not only is an advantage from mechanical properties point of view, but also encourages cells to attach and proliferate on the surface of samples. Previous investigations on other materials show that a certain level of substrate stiffness is needed for the adherence and proliferation of cells [64,65]. For instance, adhering cells on polyacrylamide gels with excessive soft surface cannot spread, and therefore go through apoptosis [64].

4. Conclusions

Biodegradable polycaprolactone fumarate (PCLF)/gelatin-based nanocomposites incorporated with the 0, 5 and 10 wt% silicon and magnesium co-doped fluorapatite nano-powder (Si-Mg-FA) were successfully synthesized via electrospinning process. The highlighted results are listed below:

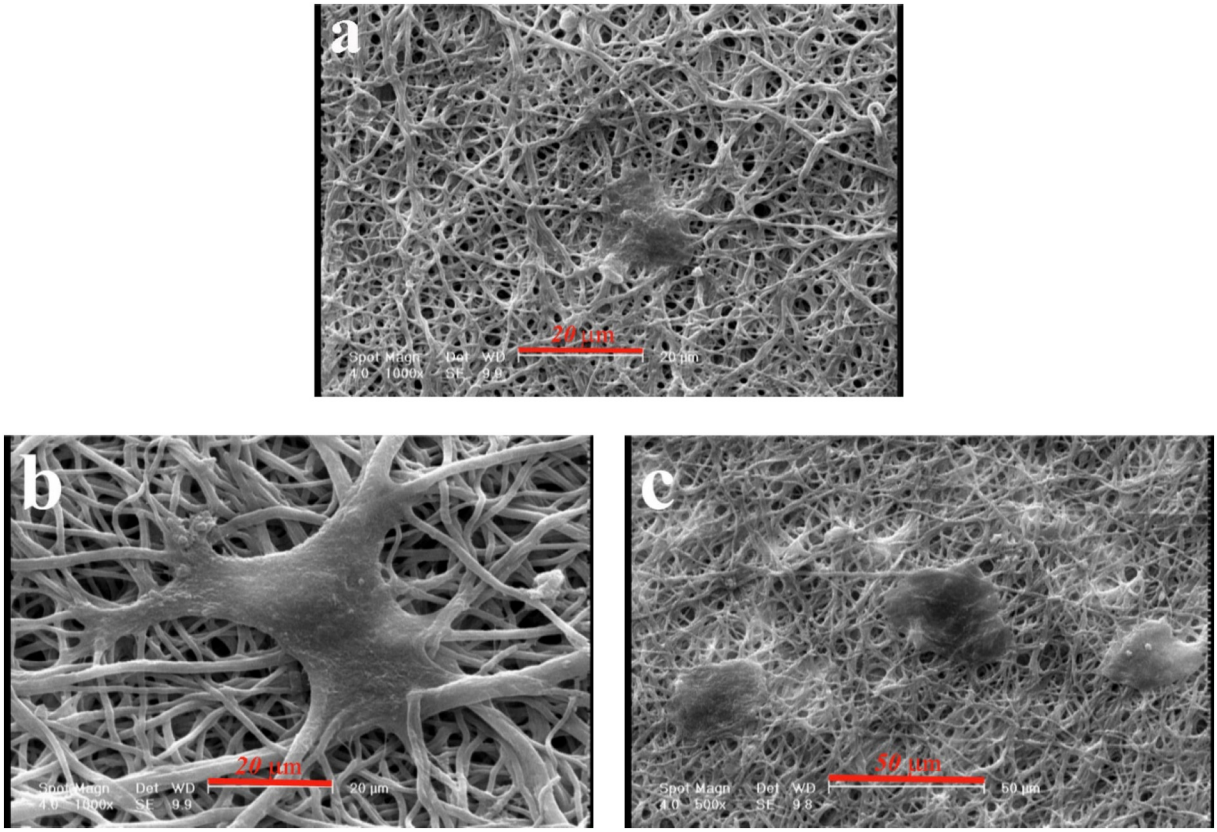

Fig. 10. SEM micrographs of L929 fibroblast cells cultured on (a) P-G membrane and (b) and (c) P-G-5NP membrane at different magnifications.

1- Incorporation of Si-Mg-FA nanoparticles resulted in reduced fiber diameter of the membranes.
2- Incorporation of 5 wt% Si-Mg-FA nanoparticles significantly improved mechanical properties of the PCLF/gelatin membrane.
3- There was no clear difference between degradation rate of PCLF/gelatin and PCLF/gelatin with 5 wt% nanoparticles at 7, 14 and 28 days of immersion in phosphate buffer saline while 10 wt% nanoparticles significantly increased biodegradation of PCLF/gelatin
4- Based on the MTT assays, the samples have no in vitro toxicity to the cells. Furthermore, although a good cell attachment occurs for all samples, the cells on the P-G-5NP nano-composite are well spread and display flattened sheet morphologies.

The results of the present investigation have demonstrated that P-G-5NP nano-composite is a potential candidate for fabricating GTR/GBR membranes due to its proper microstructure and mechanical features as well as its appropriate biodegradation and biocompatibility behaviors.

References

[1] C.C. Villar, D.L. Cochran, Regeneration of periodontal tissues: guided tissue regeneration, Dent. Clin. North Am. 54 (2010) 73–92.
[2] M. Chakraborti, J.K. Jackson, D. Plackett, D.M. Brunette, H.M. Burt, Drug intercalation in layered double hydroxide clay: application in the development of a nanocomposite film for guided tissue regeneration, Int. J. Pharm. 416 (2011) 305–313.
[3] B.L. Pihlstrom, B.S. Michalowicz, N.W. Johnson, Periodontal diseases, Lancet 366 (2005) 1809–1820.
[4] M.C. Bottino, V. Thomas, G.M. Janowski, A novel spatially designed and functionally graded electrospun membrane for periodontal regeneration, Acta Biomater. 7 (2011) 216–224.
[5] F. Yang, S.K. Both, X. Yang, X.F. Walboomers, J.A. Jansen, Development of an electrospun nano-apatite/PCL composite membrane for GTR/GBR application, Acta Biomater. 5 (2009) 3295–3304.
[6] F.M. Veronese, F. Marsilio, S. Lora, P. Caliceti, Polyphosphazene membranes and microspheres in periodontal diseases and implant surgery, Biomaterials 20 (1999) 91–98.
[7] Y. Wu, H. Xia, B. Zhang, Y. Zhao, Y. Wang, Assessment of polyglycolic acid scaffolds for periodontal ligament regeneration, Biotechnol. Biotech. Equip. 32 (2018) 701–706.
[8] H. Hong, J. Wei, C. Liu, Development of asymmetric gradational-changed porous chitosan membrane for guided periodontal tissue regeneration, Compos. B Eng. 38 (2007) 311–316.
[9] S. Zhang, Y. Huang, X. Yang, F. Mei, Q. Ma, G. Chen, S. Ryu, X. Deng, Gelatin nanofibrous membrane fabricated by electrospinning of aqueous gelatin solution for guided tissue regeneration, J. Biomed. Mater. Res. A (2008) 671–679.
[10] M.B. Runge, H. Wang, R.J. Spinner, A.J. Windebank, M.J. Yaszemski, Reformulating polycaprolactone fumarate to eliminate toxic diethylene glycol: effects of polymeric branching and autoclave sterilization on material properties, Acta Biomater. 8 (2012) 133–143.
[11] S. Sharifi, H. Mirzadeh, M. Imani, F. Ziaee, M. Tajabadi, A. Jamshidi, M. Atai, Synthesis, photocrosslinking characteristics, and biocompatibility evaluation of N-vinyl pyrrolidone/polycaprolactone fumarate biomaterials using a new proton scavenger, Polym. Adv. Technol. 19 (2008) 1828–1838.
[12] S. Sharifi, H. Mirzadeh, M. Imani, Z. Rong, Injectable in situ forming drug delivery system based on poly (ε-caprolactone fumarate) for tamoxifen citrate delivery: gelation characteristics, in vitro drug release and anti-cancer evaluation, Acta Biomater. 5 (2009) 1966–1978.
[13] J.A. Parry, E.R. Wagner, P.L. Kok, M. Dadsetan, M.J. Yaszemski, A.J. van Wijnen, S. Kakar, A combination of a polycaprolactone fumarate scaffold with polyethylene terephthalate sutures for intra-articular ligament regeneration, Tissue Eng. A 24 (2018) 1–32.
[14] S.M. Best, A.E. Porter, E.S. Thian, J. Huang, Bioceramics: past, present and for the future, J. Eur. Ceram. Soc. 28 (2008) 1319–1327.
[15] R.Z. Legeros, Apatites in biological systems, Prog. Cryst. Growth Charact. 4 (1981) 1–45.
[16] L.J. Jha, S.M. Best, J.C. Knowles, I. Rehman, J.D. Santo, W. Bonfield, Preparation and characterization of fluoride-substituted apatites, J. Mater. Sci. Mater. Med. 8 (1997) 185–191.
[17] A. Sharifnabi, M.H. Fathi, B.E. Yekta, M. Hossainalipour, The structural and biocorrosion barrier performance of Mg-substituted fluorapatite coating on 316L stainless steel human body implant, Appl. Surf. Sci. 288 (2014) 331–340.
[18] Y. Cai, S. Zhang, X. Zeng, Y. Wang, M. Qian, W. Weng, Improvement of bioactivity with magnesium and fluorine ions incorporated hydroxyapatite coatings via sol–gel deposition on Ti6Al4V alloys, Thin Solid Films 517 (2009) 5347–5351.
[19] A.E. Porter, N. Patel, J.N. Skepper, S.M. Best, W. Bonfield, Comparison of in vivo dissolution processes in hydroxyapatite and silicon-substituted hydroxyapatite bioceramics, Biomaterials 24 (2003) 4609–4620.
[20] L.L. Hench, Sol-gel Silica Properties, Processing and Technology Transfer, 1st ed., Noyes Publications, 1998, pp. 116–163.

[21] L.J. Pullen, K.A. Gross, Dissolution and mineralization of sintered and thermally sprayed hydroxy-fluoroapatites, J. Mater. Sci. Mater. Med. 16 (2005) 399–404.
[22] M.H. Fathi, E.M. Zahrani, A. Zomorodian, Novel fluorapatite/niobium composite coating for metallic human body implants, Mater. Lett. 63 (2009) 1195–1198.
[23] K. Cheng, G. Shen, W. Weng, G. Han, J.M.F. Ferreira, J. Yang, Synthesis of hydroxyapatite/fluoroapatite solid solution by a sol–gel method, Mater. Lett. 51 (2001) 37–41.
[24] M. Kheradmandfard, M.H. Fathi, F. Ansari, T. Ahmadi, Effect of Mg content on the bioactivity and biocompatibility of Mg-substituted fluorapatite nanopowders fabricated via mechanical activation, Mater. Sci. Eng. C 68 (2016) 136–142.
[25] T. Ahmadi, A. Monshi, V. Mortazavi, M.H. Fathi, B. Hashemibeni, A.A. Sharifnabi, In vitro behavior of mechanically activated nanosized Si-Mg-doped fluorapatite, Adv. Ceram. Prog. 2 (2016) 5–11.
[26] A. Jafarzadeha, T. Ahmadi, M. Taghian Dehaghani, K. Mohemi, Synthesis, corrosion and bioactivity evaluation of gelatin/silicon and magnesium co-doped fluorapatite nanocomposite coating applied on AZ31 Mg alloy, Russ. J. Non-Ferr. Met. 59 (2018) 458–464.
[27] T. Ahmadi, A. Monshi, V. Mortazavi, M.H. Fathi, S. Sharifi, B. Hashemi Beni, A. Moghare Abed, M. Kheradmandfard, A. Sharifnabi, Synthesis and dissolution behavior of nanosized silicon and magnesium co-doped fluorapatite obtained by high energy ball milling, Ceram. Int. 40 (2014) 8341–8349.
[28] S. Wang, L. Lu, J.A. Gruetzmacher, B.L. Currier, M.J. Yaszemski, Synthesis and characterizations of biodegradable and crosslinkable poly(ε-caprolactone fumarate), poly(ethylene glycol fumarate), and their amphiphilic copolymer, Biomaterials 27 (2006) 832–841.
[29] P.K. Baumgarten, Electrostatic spinning of acrylic microfibers, J. Colloid Interface Sci. 36 (1971) 71–79.
[30] J. Doshi, D.H. Reneker, Electrospinning process and applications of electrospun fibers, J. Electrost. 35 (1995) 151–160.
[31] H. Fong, I. Chun, D.H. Reneker, Beaded nanofibers formed during electrospinning, Polymer 40 (1999) 4585–4592.
[32] X. Zong, K. Kim, D. Fang, S. Ran, B.S. Hsiao, B. Chu, Structure and process relationship of electrospun bioabsorbable nanofiber membranes, Polymer 43 (2002) 4403–4412.
[33] V. Viswanathan, T. Laha, K. Balani, A. Agarwal, S. Seal, Challenges and advances in nanocomposite processing techniques, Mat. Sci. Eng. R Rep. 54 (2006) 121–285.
[34] K. Fujihara, M. Kotaki, S. Ramakrishna, Guided bone regeneration membrane made of polycaprolactone/calcium carbonate composite nano-fibers, Biomaterials 26 (2005) 4139–4147.
[35] L. Postiglione, G.D. Domenico, L. Ramaglia, S. Montagnani, S. Salzano, M. Vitale, G. Rossi, Behavior of SaOS-2 cells cultured on different titanium surfaces, J. Dent. Res. 82 (2003) 692–696.
[36] A. Wennerberg, C. Hallgren, C. Johansson, S. Danelli, A histomorphometric evaluation of screw-shaped implants each prepared with two surface roughnesses, Clin. Oral Implants Res. 9 (1998) 11–19.
[37] H. Hajiali, Sh. Shahghasempour, M.R. Naimi-Jamal, H. Peirovi, Electrospun PGA/gelatin nanofibrous scaffolds and their potential application in vascular tissue engineering, Int. J. Nanomedicine 6 (2011) 2133–2141.
[38] Z.X. Meng, Y.S. Wang, C. Ma, W. Zheng, L. Li, Y.F. Zheng, Electrospinning of PLGA/gelatin randomly-oriented and aligned nanofibers as potential scaffold in tissue engineering, Mater. Sci. Eng. C 30 (2010) 1204–1210.
[39] R.I. Gibson, W. Bonfield, Novel synthesis and characterization of an AB-type carbonate-substituted hydroxyapatite, J. Biomed. Mater. Res. 59 (2002) 697–708.
[40] D. Liu, Q. Yang, T. Troczynski, Sol–gel hydroxyapatite coatings on stainless steel substrates, Biomaterials 23 (2002) 691–698.
[41] A. Hanifi, M.H. Fathi, H. Mir Mohammad Sadeghi, J. Varshosaz, Mg^{2+} substituted calcium phosphate nanoparticles synthesis for non-viral gene delivery application, J. Mater. Sci. Mater. Med. 21 (2010) 2393–2401.
[42] L. Montazeri, J. Javadpour, M.A. Shokrgozar, Hydrothermal synthesis and characterization of hydroxyapatite and fluorhydroxyapatite nano-size powders, Biomed. Mater. 5 (2010) 1–7.
[43] M. Turkoz, A.O. Atilla, Z. Evis, Silver and fluoride doped hydroxyapatites: investigation by microstructure, mechanical and antibacterial properties, Ceram. Int. 39 (2013) 8925–8931.
[44] N. Johari, M.H. Fathi, M.A. Golozar, The effect of fluorine content on the mechanical properties of poly (ε-caprolactone)/nano-fluoridated hydroxyapatite scaffold for bone-tissue engineering, Ceram. Int. 37 (2011) 3247–3251.
[45] H. Eslami, M. Solati-Hashjin, M. Tahriri, The comparison of powder characteristics and physicochemical, mechanical and biological properties between nanostructure ceramics of hydroxyapatite and fluoridated hydroxyapatite, Mater. Sci. Eng. C 29 (2009) 1387–1398.
[46] J. Sun, Y. Huang, W. Wang, Z. Yu, A. Wang, K. Yuan, Application of gelatin as a binder for the sulfur cathode in lithium–sulfur batteries, Electrochim. Acta 53 (2008) 7084–7088.
[47] Z. Dong, Q. Wang, Y. Du, Alginate/gelatin blend films and their properties for drug controlled release, J. Membr. Sci. 280 (2006) 37–44.
[48] C.S. Ki, D.H. Baek, K.D. Gang, K.H. Lee, I.C. Um, Y.H. Park, Characterization of gelatin nanofiber prepared from gelatin–formic acid solution, Polymer 46 (2005) 5094–5102.
[49] K. Pal, A.K. Banthia, D.K. Majumdar, Preparation and characterization of polyvinyl alcohol–gelatin hydrogel membranes for biomedical applications, AAPS PharmSciTech 8 (2007) E142–E146.
[50] H. Peng, Y. Han, T. Liu, W.C. Tjiu, C. He, Morphology and thermal degradation behavior of highly exfoliated CoAl-layered double hydroxide/polycaprolactone nanocomposites prepared by simple solution intercalation, Thermochim. Acta 502 (2010) 1–7.
[51] S. Wang, M.J. Yaszemski, J.A. Gruetzmacher, L. Lu, Photo-crosslinked poly(ε-caprolactone fumarate) networks: roles of crystallinity and crosslinking density in determining mechanical properties, Polymer 49 (2008) 5692–5699.
[52] E. Andrzejewska, Photopolymerization kinetics of multifunctional monomers, Prog. Polym. Sci. 26 (2001) 605–665.
[53] J.G. Kloosterboer, Network formation by chain crosslinking photopolymerization and its applications in electronics, Adv. Polym. Sci. 84 (1988) 1–61.
[54] C.M. Chana, J.S. Wub, J.X. Li, Y.K. Cheunga, Polypropylene/calcium carbonate nanocomposites, Polymer 43 (2002) 2981–2992.
[55] S.C. Wong, A. Baji, S. Leng, Effect of fiber diameter on tensile properties of electrospun poly(ε-caprolactone), Polymer 49 (2008) 4713–4722.
[56] D. Shah, P. Maiti, D.D. Jiang, C.A. Batt, E.P. Giannelis, Effect of nanoparticle mobility on toughness of polymer nanocomposites, Adv. Mater. 17 (2005) 525–528.
[57] M. Kharaziha, M. Nikkhah, S.R. Shin, N. Annabi, N. Masoumi, A.K. Gaharwar, G. Camci-Unal, A. Khademhosseini, PGS: gelatin nanofibrous scaffolds with tunable mechanical and structural properties for engineering cardiac tissues, Biomaterials 34 (2013) 6355–6366.
[58] K. Rezwan, Q.Z. Chen, J.J. Blaker, A.R. Boccaccini, Biodegradable and bioactive porous polymer/inorganic composite scaffolds for bone tissue engineering, Biomaterials 27 (2006) 3413–3431.
[59] S. Wang, M.J. Yaszemski, A.M. Knight, J.A. Gruetzmacher, A.J. Windebank, L. Lu, Photo-crosslinked poly(ε-caprolactone fumarate) networks for guided peripheral nerve regeneration: material properties and preliminary biological evaluations, Acta Biomater. 5 (2009) 1531–1542.
[60] K.M. Woo, V.J. Chen, P.X. Ma, Nano-fibrous scaffolding architecture selectively enhances protein adsorption contributing to cell attachment, J. Biomed. Mater. Res. 67A (2003) 531–537.
[61] Y. Huang, S. Onyeri, M. Siewe, A. Moshfeghian, S.V. Madihally, In vitro characterization of chitosan–gelatin scaffolds for tissue engineering, Biomaterials 26 (2005) 7616–7627.
[62] D. Liang, B.S. Hsiao, B. Chu, Functional electrospun nanofibrous scaffolds for biomedical applications, Adv. Drug Deliv. Rev. 59 (2007) 1392–1412.
[63] J.E. Gougha, J.R. Jones, L.L. Hench, Nodule formation and mineralization of human primary osteoblasts cultured on a porous bioactive glass scaffold, Biomaterials 25 (2004) 2039–2046.
[64] C.C. Yeh, C.N. Chen, Y.T. Li, C.W. Chang, M.Y. Cheng, H.I. Chang, The effect of polymer molecular weight and UV radiation on physical properties and bioactivities of PCL films, Cell. Polym. 30 (2011) 227–242.
[65] S. Wang, D.H.R. Kempen, M.J. Yaszemski, L. Lu, The roles of matrix polymer crystallinity and hydroxyapatite nanoparticles in modulating material properties of photo-crosslinked composites and bone marrow stromal cell responses, Biomaterials 30 (2009) 3359–3370.